RAA 2020 Vol. **20** No. **8**, 125(13pp) doi: 10.1088/1674–4527/20/8/125

http://www.raa-journal.org *http://iopscience.iop.org/raa*

***R**esearch in*
***A**stronomy and*
***A**strophysics*

Detection of hydroxyacetone in protostar IRAS 16293–2422 B

Yan Zhou[1,2], Dong-Hui Quan[2,3], Xia Zhang[2] and Sheng-Li Qin[1]

[1] Department of Astronomy, Yunnan University, and Key Laboratory of Astroparticle Physics of Yunnan Province, Kunming 650091, China; *slqin@bao.ac.cn*
[2] Xinjiang Astronomical Observatory, Chinese Academy of Sciences, Urumqi 830011, China
[3] Department of Chemistry, Eastern Kentucky University, Richmond, KY 40475, USA

Received 2020 February 15; accepted 2020 April 17

Abstract Hydroxyacetone (CH_3COCH_2OH) is one of the smallest molecules that contain both hydroxyl and carbonyl group on neighboring carbon atoms. This steric configuration is characteristic of saccharides and determines their biochemical activity. The attempt to search for hydroxyacetone toward the massive star formation region Sagittarius B2(N) was unsuccessful. Here we report the first detection of CH_3COCH_2OH in the solar-type protostar IRAS 16293–2422 B, using the Atacama Large Millimeter Array science verification data at Band 4. In a total of 11 unblended transitions of CH_3COCH_2OH with upper level energies ranging from 86 to 246 K are identified. From our local thermodynamic equilibrium analysis, we derived that the rotational temperature of CH_3COCH_2OH is 160±21 K and the column density is (1.2±1.0) $\times 10^{16}$ cm^{-2}, which results in a fractional abundance of 7×10^{-10} with respect to molecular hydrogen. In this work, we present the identification of CH_3COCH_2OH in IRAS 16293–2422 B and propose a simple formation mechanism. The unambiguous identification of hydroxyacetone may provide the basis for future study of the origin and evolution of saccharides in the interstellar medium.

Key words: ISM: abundances — ISM: individual (IRAS 16293–2422 B) — ISM: molecules

1 INTRODUCTION

The carbohydrates have caused increasing interests of astrophysical studies in recent years because these molecules can serve as energy storage[1], can participate in the building of DNA and RNA, and are structural elements in cellular molecular organization (e.g., cell membranes) (Mohăcek-Groše 2005). They can also form sophisticated extracellular matrices throughout the organism (Iozzo 1998). Therefore, carbohydrates are vital to all known lifeforms (Cooper et al. 2001). All monosaccharides show common structural feature that carbonyl group occurs next to hydroxyl group in the chain conformation of sugar molecules (Mohăcek-Groše 2005). Examples of the smallest sugar molecules are glycolaldehyde $HCOCH_2OH$ and hydroxyacetone CH_3COCH_2OH. Searching for the monosaccharides in interstellar medium (ISM) has caused considerable interest, as the existence and the process to form these molecules in ISM may help with answering the question of the origin and evolution of life in the universe (Bossa et al. 2014).

Glycolaldehyde $HCOCH_2OH$ has been studied intensively in various sources. The glycolaldehyde was firstly detected toward the Galactic Center (Hollis et al. 2000, 2001, 2004a; Halfen et al. 2006; Requena-Torres et al. 2008). Then it was detected in a number of other places in ISM, associated with the star formation regions of high (Beltrán et al. 2009; Calcutt et al. 2014), intermediate (Fuente et al. 2014) and low mass (Jørgensen et al. 2012; Coutens et al. 2015; Taquet et al. 2015; Jørgensen et al. 2016). It was also detected in comet C/2014 Q2 (Lovejoy) (Biver et al. 2015).

Hydroxyacetone CH_3COCH_2OH, compared with glycolaldehyde $HCOCH_2OH$, exhibits the next level of molecular complexity among the smallest sugar molecules (Apponi et al. 2006a). In laboratory, this molecule is an important starting material in the synthesis of aldehydes and ketones (see, e.g., Solomons 1984). Therefore, the assumption that such molecule could lead to the production of complex prebiotic species in ISM should be plausible (Apponi et al. 2006b). Two searches for hydroxyacetone toward Sagittarius B2(N) (hereafter Sgr B2(N)) were

[1] The energy discussed here is the energy sustaining the vital activities of body, such as blood circulation, digestion and absorption of the stomach and so on.

conducted with non-detection of the molecule. The first attempt was at 1.3 mm using the Caltech Submillimeter Observatory (CSO), with no detected transitions of hydroxyacetone (Braakman et al. 2010). The second attempt was at 3 mm using the Arizona Radio Observatory (ARO) 12 m telescope. Although there are several coincidental transitions matching CH_3COCH_2OH lines, the absence of several favorable transitions indicates that the result is not enough for claiming a detection (Apponi et al. 2006b). The aim of our study is to present a reliable identification of CH_3COCH_2OH with the highly sensitive Atacama Large Millimeter Array (ALMA) at Band 4, toward a typical young solar-type protostar IRAS 16293–2422 B (hereafter I16293B).

The class 0 protostar IRAS 16293–2422 (hereafter I16293) contains at least two sources, A and B, with a separation of 5″ (∼700 AU) (Calcutt et al. 2018). Many line surveys have been carried out towards I16293 by using single dish telescopes and interferometers (Cazaux et al. 2003; Bisschop et al. 2008; Caux et al. 2011; Jørgensen et al. 2016; Lykke et al. 2017; Martín-Doménech et al. 2017). The results show that I16293 exhibits a rich chemistry and chemical complexity of complex organic molecules (COMs). There are many oxygen-bearing COMs that have been detected in I16293. Examples are glycolaldehyde, ethanol, ethylene glycol, acetic acid, propanal and others, which are reported by the Protostellar Interferometric Line Survey (PILS) studies (e.g., Jørgensen et al. 2012, 2016; Lykke et al. 2017; Jørgensen et al. 2018). Since the hydroxyacetone closely resembles glycolaldehyde, I16293 is very likely to be a source to search for hydroxyacetone.

In this work, we report the identification of hydroxyacetone at the 2 mm waveband toward I16293B. We describe the observations in Section 2, and present the results and analyze the data in Sections 3 and 4, respectively. We draw a few conclusions in Section 5.

2 OBSERVATIONS

We took the uncalibrated data from the ALMA science verification (SV) program toward I16293 at Band 4[2]. We downloaded and re-calibrated the data using the standard ALMA calibration scripts. These data were obtained by observations that were carried out with 23×12 m antennas on 2014 July 14. The primary beam size at Band 4 is about 30″. The phase-tracking center is at R.A.(J2000) = $16^h32^m22.73^s$ and decl.(J2000) = $-24°28'32.50''$. There are four spectral windows with 3840 channels each. These four spectral windows cover frequency ranging from 145.1 to 159.2 GHz, with spectral resolutions from 0.06 to 0.49 MHz. We did the follow-up calibration and imaging employing the CASA software[3]. We have flagged the first and last 20 channels to avoid the edge problem. We processed the continuum-subtraction with STATCONT software (Sánchez-Monge et al. 2018).

The continuum image is constructed from line-free channel as shown in color scale in Figure 2. The peak intensity of I16293B is 0.35±0.006 Jy beam^{-1}, and the synthesized beam size is $1.04'' \times 0.59''$. Therefore, the beam averaged H_2 column density is derived to be 1.7×10^{25} cm^{-2} for I16293B (Lis et al. 1991). The result is similar to the H_2 column density calculated by Martín-Doménech et al. (2017) and Jørgensen et al. (2016) toward I16293B.

3 RESULTS

In IRAS 16293–2422 A, the lines are quite broad, leading to significant line confusion that prevents the search for complex species (e.g., Jørgensen et al. 2012). This report is therefore focusing on source B only. Full band spectra[4] are extracted at the continuum peak position of source B. The eXtended CASA Line Analysis Software Suite (XCLASS) (Möller et al. 2017) package[5] is employed for identifying line transitions under the assumption of local thermodynamical equilibrium (LTE)[6], and is used to access database Cologne Database for Molecular Spectroscopy (CDMS) (Müller et al. 2001, 2005; `http://cdms.de`) as well as the Jet Propulsion Laboratory (JPL) database (Pickett et al. 1998; `http://spec.jpl.nasa.gov`). For hydroxyacetone, the JPL database is used to access the XCLASS package. The spectroscopic data of CH_3COCH_2OH, with the A and E torsional states, has been studied by Kattija-Ari & Harmony (1980) (from 4 to 180 GHz), and more recently by Apponi et al. (2006b) (from 4 to 180 GHz) and Braakman et al. (2010) (near 300 GHz). Since the spectra of I16293B are really rich, a careful check should be done to avoid blended or overlapped line problems. To achieve this, we have made a full source model (coded in solid green color in Fig. B.1 of Appendix) including as many species to model the observed spectra toward I16293B. The species which were observed in I16293B up to now (from table 1 by Drozdovskaya et al. 2019) are all included in the full source model.

[2] Obtaining ALMA data and calibration scripts: `https://almascience.nrao.edu/almadata/sciver/IRAS16293Band4/`

[3] CASA homepage: `http://casa.nrao.edu`

[4] Fig. 1 shows the unblended or partially blended emission lines of hydroxyacetone toward I16293B. Full band spectra are presented in Fig. B.1, which are populated by many molecular lines.

[5] The spectroscopic database contained in XCLASS is interfacing with Virtual Atomic and Molecular Data Centre (VAMDC): `http://www.vamdc.org/activities/research/`

[6] LTE is a good assumption in this case, because the densities are high at the chosen position and thus the molecules are expected to be thermalized.

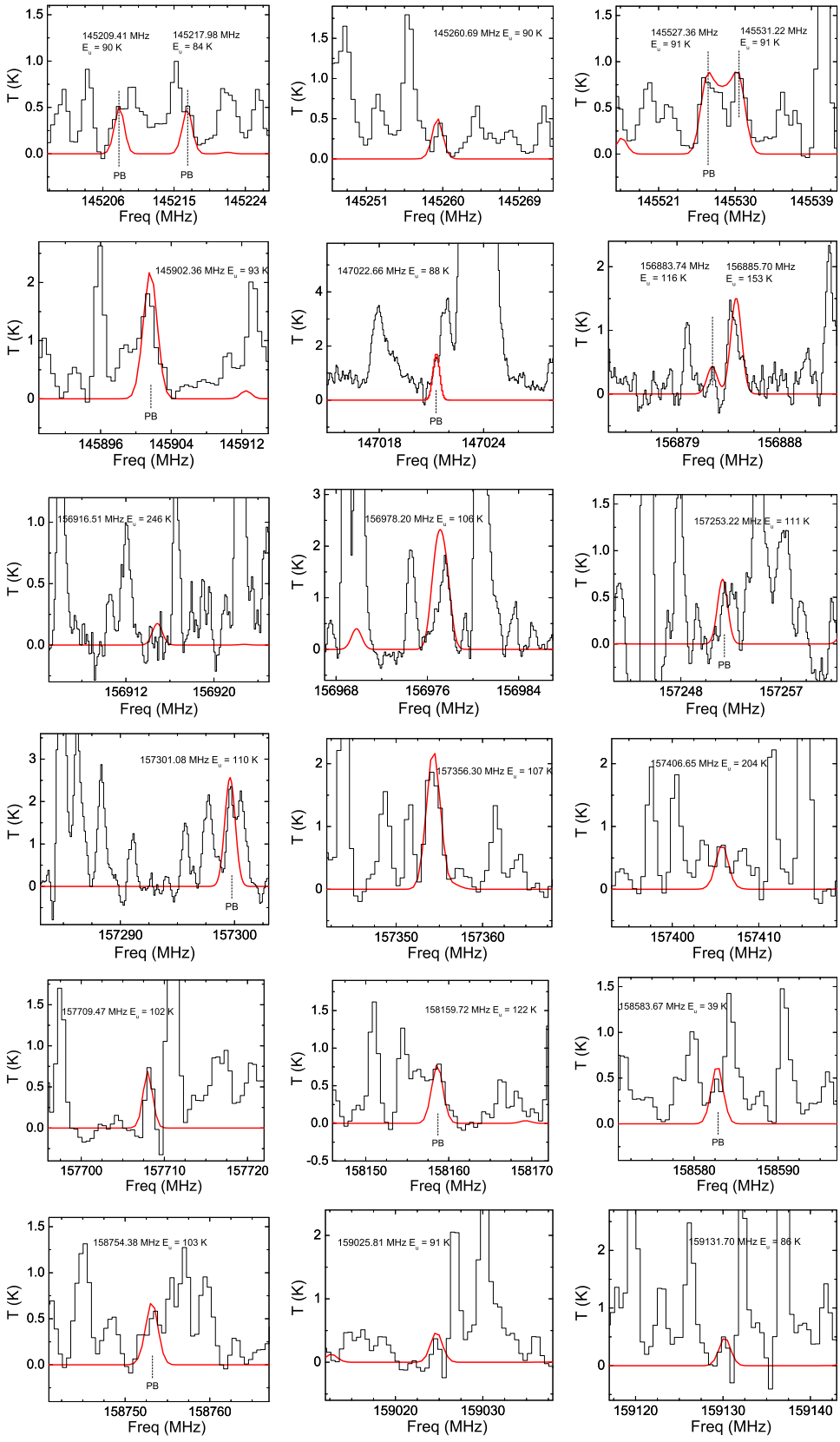

Fig. 1 The unblended and partially blended (denoted with "PB") lines of hydroxyacetone detected in these four spectral windows at Band 4 toward I16293B overlaid with an LTE spectral model of the emission.

Table 1 Observed Spectral Line Parameters of Detected Species CH_3COCH_2OH toward I16293B

Rest Frequency (MHz) (1)	Uncertainty (MHz) (2)	Einstein A (10^{-5} s^{-1}) (3)	E_u (K) (4)	$g_{\rm up}$ (5)	Quantum Numbers (6)	$V_{\rm LSR}$ (km s^{-1}) (7)	ΔV (km s^{-1}) (8)	I_P (K) (9)	σ (K) (10)	Detection Level (11)	Notes (12)
145141.73	0.05	7.49	90	94	22(3,20)– 23(2,21)A	...	...	...	...	...	B
145209.41	0.05	5.58	90	94	22(3,20)– 23(3,21)A	...	...	...	...	...	PB
145217.98	0.68	3.69	84	66	16(10,6)– 16(11,5)A	...	...	...	...	...	PB
145217.98	0.68	3.69	84	66	16(10,7)– 16(11,6)A	...	...	...	...	...	b
145237.27	0.40	4.24	228	150	36(4,32)– 36(5,31)A	...	...	...	...	...	B
145260.69	0.05	5.58	90	94	22(2,20)– 23(2,21)A	2.500 $\pm$ 0.022	2.895 $\pm$ 0.020	0.591	0.070	8 σ	D
145304.16	0.05	9.27	94	49	23(2,22)– 24(1,23)E	...	...	...	...	...	B
145306.59	0.05	9.27	94	49	23(1,22)– 24(2,23)E	...	...	...	...	...	B
145328.44	0.05	7.52	90	94	22(2,20)– 23(3,21)A	...	...	...	...	...	B
145351.01	0.68	3.35	79	62	15(10,5)– 15(11,4)A	...	...	...	...	...	B
145351.01	0.68	3.35	79	62	15(10,6)– 15(11,5)A	...	...	...	...	...	b
145424.05	0.41	4.25	228	150	36(5,32)– 36(6,31)A	...	...	...	...	...	B
145462.03	0.69	2.94	74	58	14(10,5)– 14(11,4)A	...	...	...	...	...	B
145462.03	0.69	2.94	74	58	14(10,4)– 14(11,3)A	...	...	...	...	...	b
145527.36	0.05	9.11	91	98	23(2,22)– 24(1,23)A	...	...	...	...	...	PB
145528.71	0.05	5.70	91	98	23(2,22)– 24(2,23)A	...	...	...	...	...	B
145529.92	0.05	5.70	91	98	23(1,22)– 24(1,23)A	...	...	...	...	...	b
145531.22	0.05	9.11	91	98	23(1,22)– 24(2,23)A	2.443 $\pm$ 0.041	2.747 $\pm$ 0.040	1.126	0.068	17 σ	D
145553.78	0.69	2.44	70	54	13(10,4)– 13(11,3)A	...	...	...	...	...	B
145553.78	0.69	2.44	70	54	13(10,3)– 13(11,2)A	...	...	...	...	...	b
145597.03	0.35	0.25	172	130	32(3,30)– 32(3,29)A	...	...	...	...	...	B
145597.33	0.35	2.82	172	130	32(2,30)– 32(3,29)A	...	...	...	...	...	b
145604.76	0.35	2.82	172	130	32(3,30)– 32(4,29)A	...	...	...	...	...	B
145605.07	0.35	0.25	172	130	32(2,30)– 32(4,29)A	...	...	...	...	...	b
145628.77	0.69	1.81	66	50	12(10,3)– 12(11,2)A	...	...	...	...	...	B
145628.77	0.69	1.81	66	50	12(10,2)– 12(11,1)A	...	...	...	...	...	b
145677.39	0.91	6.52	289	150	38(11,28)– 38(12,27)A	...	...	...	...	...	B
145730.23	0.05	5.56	87	90	21(3,18)– 22(3,19)A	...	...	...	...	...	B
145805.54	0.37	3.60	199	140	34(3,31)– 34(4,30)A	...	...	...	...	...	B
145815.58	0.93	6.46	277	150	37(11,26)– 37(12,25)A	...	...	...	...	...	B
145845.63	0.05	5.15	95	51	24(1,24)– 25(1,25)E	...	...	...	...	...	B
145845.63	0.05	5.15	95	51	24(0,24)– 25(0,25)E	...	...	...	...	...	b
145845.63	0.05	11.22	95	51	24(1,24)– 25(0,25)E	...	...	...	...	...	b
145845.63	0.05	11.22	95	51	24(0,24)– 25(1,25)E	...	...	...	...	...	b
145902.36	0.05	10.64	93	100	24(1,24)– 25(0,25)A	...	...	...	...	...	PB
145902.36	0.05	5.75	93	100	24(1,24)– 25(1,25)A	...	...	...	...	...	b
145902.36	0.05	5.75	93	100	24(0,24)– 25(0,25)A	...	...	...	...	...	b
145902.36	0.05	10.64	93	100	24(0,24)– 25(1,25)A	...	...	...	...	...	b
146048.18	0.05	5.88	89	45	21(3,18)– 22(4,19)E	...	...	...	...	...	B
146220.81	0.05	5.27	85	43	20(4,16)– 21(4,17)E	...	...	...	...	...	B
146369.91	0.53	5.91	338	170	43(8,36)– 43(9,35)A	...	...	...	...	...	B
146517.87	0.02	5.03	89	43	20(6,15)– 21(6,16)E	...	...	...	...	...	B
146686.58	0.05	4.03	98	94	22(5,18)– 23(4,19)A	...	...	...	...	...	B
146726.58	0.12	4.00	38	54	12(4,8)– 13(5,9)A	...	...	...	...	...	B
146828.51	0.44	5.45	303	170	41(6,35)– 41(7,34)A	...	...	...	...	...	B
147022.66	0.05	5.48	88	86	20(6,14)– 21(6,15)A	...	...	...	...	...	PB
147081.70	0.19	6.01	188	59	29(11,19)– 29(12,18)E	...	...	...	...	...	B
156883.74	0.08	5.99	116	47	23(9,15)– 22(9,14)E	2.931 $\pm$ 0.051	2.799 $\pm$ 0.094	0.549	0.118	5 σ	D
156885.70	0.79	6.47	153	100	25(11,14)– 25(12,13)A	2.963 $\pm$ 0.055	2.215 $\pm$ 0.068	1.178	0.126	9 σ	D
156885.98	0.79	6.47	153	100	25(11,15)– 25(12,14)A	...	...	...	...	...	b
156901.46	0.05	6.44	37	50	11(5,6)– 12(6,7)A	...	...	...	...	...	B
156916.51	1.16	1.77	246	150	36(9,27)– 35(10,26)A	2.997 $\pm$ 0.080	2.321 $\pm$ 0.090	0.161	0.130	1 σ	D
156971.26	0.24	11.41	36	19	8(7,2)– 9(8,2)E	...	...	...	...	...	B
156978.20	0.05	11.61	106	110	25(2,24)– 26(1,25)A	2.478 $\pm$ 0.048	2.214 $\pm$ 0.056	2.107	0.122	17 σ	D
156978.71	0.05	7.22	106	110	25(2,24)– 26(2,25)A	...	...	...	...	...	b
156978.71	0.05	7.22	106	110	25(1,24)– 26(1,25)A	...	...	...	...	...	b
156979.27	0.05	11.61	106	110	25(1,24)– 26(2,25)A	...	...	...	...	...	b
157034.01	0.05	6.45	37	50	11(5,7)– 12(6,6)A	...	...	...	...	...	B
157253.22	0.05	6.42	111	94	22(8,15)– 23(8,16)A	...	...	...	...	...	PB
157266.79	0.79	6.34	144	98	24(11,13)– 24(12,12)A	...	...	...	...	...	B
157266.90	0.79	6.34	144	98	24(11,14)– 24(12,13)A	...	...	...	...	...	b
157301.08	0.05	16.42	110	55	26(0,26)– 27(1,27)E	...	...	...	...	...	PB
157301.08	0.05	16.42	110	55	26(1,26)– 27(0,27)E	...	...	...	...	...	b
157301.08	0.05	4.20	110	55	26(0,26)– 27(0,27)E	...	...	...	...	...	b
157301.08	0.05	4.20	110	55	26(1,26)– 27(1,27)E	...	...	...	...	...	b

Table 1 *Continued.*

Rest Frequency (MHz) (1)	Uncertainty (MHz) (2)	Einstein A (10^{-5} s^{-1}) (3)	E_u (K) (4)	$g_{\rm up}$ (5)	Quantum numbers (6)	$V_{\rm LSR}$ (km s^{-1}) (7)	ΔV (km s^{-1}) (8)	I_P (K) (9)	σ (K) (10)	Detection Level (11)	Notes (12)
157356.30	0.05	13.42	107	110	26(1,26)– 27(0,27)A	2.400 ± 0.014	2.540 ± 0.054	2.088	0.063	33 σ	D
157356.30	0.05	7.24	107	110	26(1,26)– 27(1,27)A	...	...	...	...	...	b
157356.31	0.05	7.24	107	110	26(0,26)– 27(0,27)A	...	...	...	...	...	b
157356.31	0.05	13.42	107	110	26(0,26)– 27(1,27)A	...	...	...	...	...	b
157378.30	0.05	7.85	101	98	23(3,20)– 24(4,21)A	...	...	...	...	...	B
157406.65	0.26	0.28	204	71	35(3,33)– 35(3,32)E	2.540 ± 0.065	2.265 ± 0.026	0.493	0.063	8 σ	D
157406.66	0.26	3.26	204	71	35(2,33)– 35(3,32)E	...	...	...	...	...	b
157407.33	0.05	6.44	111	94	22(8,14)– 23(8,15)A	...	...	...	...	...	b
157407.45	0.26	3.26	204	71	35(3,33)– 35(4,32)E	...	...	...	...	...	b
157407.46	0.26	0.28	204	71	35(2,33)– 35(4,32)E	...	...	...	...	...	b
157504.29	0.05	6.70	100	47	22(4,18)– 23(4,19)E	...	...	...	...	...	B
157560.49	0.05	7.01	92	90	21(5,16)– 22(5,17)A	...	...	...	...	...	B
157603.43	0.79	6.19	137	94	23(11,12)– 23(12,11)A	...	...	...	...	...	B
157603.47	0.79	6.19	137	94	23(11,13)– 23(12,12)A	...	...	...	...	...	b
157689.00	0.22	8.95	34	42	9(6,3)– 10(7,4)A	...	...	...	...	...	B
157689.35	0.22	8.95	34	42	9(6,4)– 10(7,3)A	...	...	...	...	...	b
157709.47	0.05	6.86	102	94	22(6,17)– 23(6,18)A	2.770 ± 0.033	2.770 ± 0.087	0.745	0.062	12 σ	D
157845.78	0.05	4.10	52	66	15(4,11)– 16(5,12)A	...	...	...	...	...	B
157899.80	0.79	6.02	129	90	22(11,11)– 22(12,10)A	...	...	...	...	...	B
157899.82	0.79	6.02	129	90	22(11,12)– 22(12,11)A	...	...	...	...	...	b
157965.41	0.05	6.72	106	94	22(7,16)– 23(7,17)A	...	...	...	...	...	B
157981.52	0.53	0.23	123	51	25(4,21)– 25(7,19)E	...	...	...	...	...	B
157982.08	0.03	6.67	109	47	22(7,15)– 23(7,16)E	...	...	...	...	...	b
158144.94	0.05	12.81	32	34	7(7,1)– 8(8,0)A	...	...	...	...	...	B
158144.94	0.05	12.81	32	34	7(7,0)– 8(8,1)A	...	...	...	...	...	b
158159.72	0.80	5.81	122	86	21(11,10)– 21(12,9)A	...	...	...	...	...	PB
158159.73	0.80	5.81	122	86	21(11,11)– 21(12,10)A	...	...	...	...	...	b
158386.69	0.80	5.58	115	82	20(11,9)– 20(12,8)A	...	...	...	...	...	B
158386.69	0.80	5.58	115	82	20(11,10)– 20(12,9)A	...	...	...	...	...	b
158477.02	0.12	4.41	42	58	13(4,10)– 14(5,9)A	...	...	...	...	...	B
158583.67	0.06	2.18	39	58	13(3,11)– 14(4,10)A	...	...	...	...	...	PB
158583.92	0.80	5.30	109	78	19(11,8)– 19(12,7)A	...	...	...	...	...	b
158583.92	0.80	5.30	109	78	19(11,9)– 19(12,8)A	...	...	...	...	...	b
158709.92	0.05	7.16	97	94	22(4,18)– 23(4,19)A	...	...	...	...	...	B
158710.03	0.40	7.86	247	69	34(12,23)– 34(13,22)E	...	...	...	...	...	b
158754.38	0.81	4.98	103	74	18(11,7)– 18(12,6)A	...	...	...	...	...	PB
158754.38	0.81	4.98	103	74	18(11,8)– 18(12,7)A	...	...	...	...	...	b
158863.69	0.90	8.32	322	160	40(12,28)– 40(13,27)A	...	...	...	...	...	B
158900.83	0.81	4.61	97	70	17(11,6)– 17(12,5)A	...	...	...	...	...	B
158900.83	0.81	4.61	97	70	17(11,7)– 17(12,6)A	...	...	...	...	...	b
159025.81	0.82	4.16	91	66	16(11,6)– 16(12,5)A	2.570 ± 0.032	2.478 ± 0.054	0.428	0.078	5 σ	D
159025.81	0.82	4.16	91	66	16(11,5)– 16(12,4)A	...	...	...	...	...	b
159131.70	0.82	3.63	86	62	15(11,5)– 15(12,4)A	2.580 ± 0.049	2.376 ± 0.053	0.514	0.077	7 σ	D
159131.70	0.82	3.63	86	62	15(11,4)– 15(12,3)A	...	...	...	...	...	b

[b]Blend with each other. Transitions with higher Einstein coefficient A and lower energy level have the more contribution to the intensity of spectrum. [D]The detected unblended transitions of CH_3COCH_2OH. [PB]Partially blended with nearby transitions.

3.1 Detection of the Hydroxyacetone

We identified a total of 11 unblended emission lines of CH_3COCH_2OH with upper-level energies ranging from 86 to 246 K, among which 10 transitions have line-strength higher than 5σ. The σ is the rms noise level of the specific lines. We determined the rms noise level from emission free regions of the channel maps. The unblended or partially blended synthetic spectra for CH_3COCH_2OH toward I16293B are generated and shown in Figure 1, and the corresponding parameters for these individual detected lines are listed in Table 1. The full spectra of CH_3COCH_2OH at Band 4 are presented in Figure B.1 in the Appendix. The transitions which are higher than 3σ and totally blended with other molecules are denoted with "B" in Figure B.1. The frequencies of CH_3COCH_2OH totally blended transitions with peak intensities lower than 3σ are listed in Table A.1 and presented in Figure B.1 denoted with "w" in the Appendix. We made the Gaussian fitting to unblended transitions and obtained the parameters $V_{\rm LSR}$ and ΔV for each individual unblended transitions as shown in Columns (7)–(8) in Table 1. The averaged $V_{\rm LSR}$ value is 2.65±0.045 km s^{-1}. The averaged line width obtained from the eleven unblended transitions is 2.51±0.058 km s^{-1}. Our results of $V_{\rm LSR}$ and ΔV are consistent with previous results of other molecules in I16293B (Caux et al. 2011; Jørgensen et al. 2011). The spatial distribution of CH_3COCH_2OH is shown in Figure 2 and it is well coincident with the continuum emission of source B.

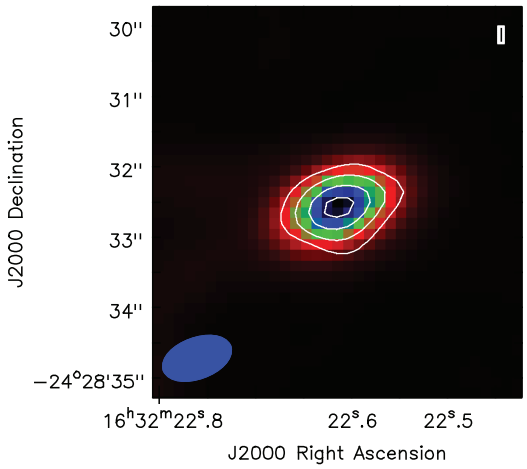

Fig. 2 Integrated intensity maps of representative CH_3COCH_2OH unblended lines observed towards I16293B. The color scale is the continuum of I16293B. The white contours indicate 5, 30, 60 and 90 percent of the total integrated intensity at a rest frequency of 157356.303 MHz. The E_u of the transitions is 107 K, and integrated velocity range is 1 to 5 km s^{-1}. Beam size is shown in the bottom left-hand corner.

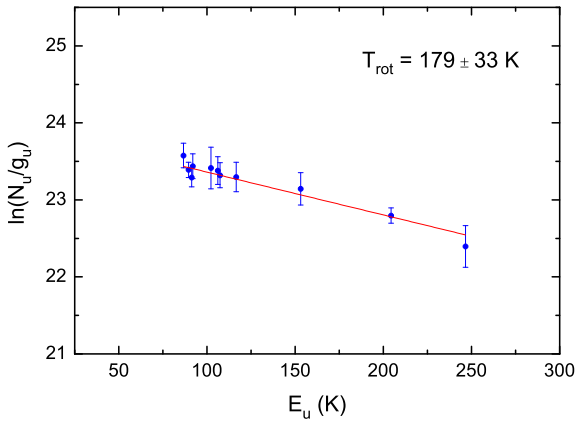

Fig. 3 Rotation temperature diagram for CH_3COCH_2OH. The *filled circles* are for the observed transitions. The *vertical bars* indicate the 3σ errors. A linear least-squares fit is shown as the *red solid line*.

The source size is derived by performing two-dimensional Gaussian fitting to the line images. The source size of CH_3COCH_2OH is unresolved. The compact source size of CH_3COCH_2OH is consistent with the other COMs detected in previous studies (e.g., Martín-Doménech et al. 2017) or PILS papers (e.g., Jørgensen et al. 2016; Calcutt et al. 2018; Coutens et al. 2019) toward I16293B.

The detected transitions of CH_3COCH_2OH are well reproduced by a rotational temperature of $T_{rot} = 160 \pm 21$ K. The derived T_{rot} agrees with the reported rotational temperature of other COMs detected in PILS studies, such as methyl isocyanide in I16293B (Calcutt et al. 2018). We derived that the column density is $(1.2\pm1.0)\times10^{16}$ cm^{-2} for CH_3COCH_2OH. The fractional abundance of CH_3COCH_2OH relative to H_2 is 7×10^{-10}. The column density (1.2×10^{16} cm^{-2}) of CH_3COCH_2OH is lower than that of glycolaldehyde (3.2×10^{16} cm^{-2}) detected in I16293B by PILS data Jørgensen et al. (2012). Our result is consistent with the previous report discussed by Apponi et al. (2006b) – column densities roughly follow a monotonic decrease from glycolaldehyde to hydroxyacetone.

To verify the calculated results from the XCLASS, we have made rotational temperature diagram (RTD) based on the 11 unblended transitions. Under the LTE assumption, the population of a certain energy level will follow the Boltzmann distribution. Assuming that the line emissions in question are optically thin, we fitted the 11 unblended transitions by using the least-squares method as done by Qin et al. (2010). The RTD for these unblended CH_3COCH_2OH lines from I16293B is shown in Figure 3. The RTD yields a rotational temperature of 179±33 K. Considering the errors, the result agrees reasonably well with the value of 160±21 K derived by the XCLASS package.

4 DISCUSSION

There are a number of compact organic molecules considered to be the potential precursors of biological molecules. The most well studied among these molecules are [C_2, H_4, O_2] family, for example, acetic acid (CH_3COOH). Acetic acid shares the C–C=O(OH) backbone with the simplest amino acid glycine (NH_2CH_2COOH), from which acetic acid differs only by an amino group (–NH_2) (Bergantini et al. 2018). Another example is glycolaldehyde ($HCOCH_2OH$), a diose and the simplest sugar-related specie (Hollis et al. 2000). The more complex molecules in the [C_3, H_6, O_3] family have not been detected in ISM, which include the simplest three-carbon aldehyde sugar glyceraldehyde ($CH(O)CH(OH)CH_2OH$; Hollis et al. 2004b) and ketose sugar dihydroxyacetone ($CH_2OHCOCH_2OH$; hereafter DHA; Apponi et al. 2006a). Therefore, searches for species in the [C_3, H_6, O_2] family with complexity in between [C_2, H_4, O_2] and [C_3, H_6, O_3] families might prove significant in understanding the lack of detection of the latter in the ISM. The detection and analysis of [C_3, H_6, O_2] family species may serve as a probe for the next step to understand the formation mechanism of biological molecules in ISM.

Glycolaldehyde ($HCOCH_2OH$), which belongs to the [C_2, H_4, O_2] family, can be produced by the recombination of two free radicals HCO and CH_2OH on the grain surface in ISM (Öberg et al. 2009; Butscher et al. 2015; Fedoseev et al. 2015; Chuang et al. 2016; Fedoseev et al.

2017). The reactive intermediates CH_2OH and HCO are formed through irradiation of CH_3OH-rich ices by various energetic particles (including protons, electrons, X-rays, UV photons, etc.) on the grain surface (Öberg et al. 2009). In addition, the intermediate radical CH_2OH was proposed to be formed by the H_2CO to CH_3OH hydrogenation processes ($H_2CO + H \longrightarrow CH_2OH$, $CH_2OH + H \longrightarrow CH_3OH$) (Butscher et al. 2015; Chuang et al. 2016), possibly at 15 K. Among the six of the lowest-energy members in the [C_3, H_6, O_2] family (species including propionic acid, methyl acetate, ethyl formate, hydroxyacetone, lactaldehyde, and methoxyacetaldehyde; reported in Kolesniková et al. (2018) and Alonso et al. (2019)), the hydroxyacetone (CH_3COCH_2OH) is a structural intermediate between glycolaldehyde ($HCOCH_2OH$) and the DHA ($CH_2OHCOCH_2OH$) (Braakman et al. 2010). And the hydroxyacetone ($CH_3[COCH_2OH]$) shares the O=C–C(H_2OH) backbone with the simplest sugar-related species glycolaldehyde (H[$COCH_2OH$]), from which hydroxyacetone differs only by a methyl group –CH_3. Since the structure of hydroxyacetone and glycolaldehyde is closely related, they may be formed in a similar manner. Therefore, we propose a reaction route of hydroxyacetone ($CH_2OHCOCH_2$) similar to that of glycolaldehyde ($HCOCH_2OH$), where hydroxyacetone ($CH_2OHCOCH_2$) might be formed upon recombination of two free radicals on the grain surface at low temperature as the following:

$$CH_3CO + CH_2OH \longrightarrow CH_3COCH_2OH. \quad (1)$$

The intermediate radical CH_2OH maybe induced through UV-irradiation of CH_3OH-rich ices ($CH_3OH + UV \longrightarrow CH_2OH + H$), or hydrogenation process of H_2CO to CH_3OH ($H_2CO + H \longrightarrow CH_2OH$) as mentioned before. The other intermediate radical CH_3CO are formed through the hydrogenation process of ketene ($H_2CCO + H \longrightarrow CH_3CO$) on the grain surface as reported by Michael et al. (1979) and Ruaud et al. (2015). This reaction suggests an effective chemical formation pathway of the hydroxyacetone. Thus, we propose that the hydroxyacetone can be formed upon the recombination of CH_2OH and CH_3CO on the grain surface for the first time.

At low temperature, the COMs are considered to be formed through free radicals' recombination on the grain surface as discussed above (Fedoseev et al. 2015; Chuang et al. 2016; Fedoseev et al. 2017). As the temperature increases when the source evolves, the species with lower binding energies formed on the dust grains can be evaporated into the gas phase thus complex molecules with relatively low binding energies are observable. In the gas phase, the complex molecules can also be produced by the reactions between cations and the complex molecules' precursors that are evaporated from dust grains, followed by recombination with electrons, as proposed in Remijan et al. (2002), Garrod (2013) and Redondo et al. (2017). Thus, we propose a novel gas phase production route of CH_3COCH_2OH as the other COMs:

$$CH_3COOH_2^+ + CH_3OH \longrightarrow CH_3COCH_2OH_2^+ + H_2O, \quad (2)$$

$$CH_3COCH_2OH_2^+ + e^- \longrightarrow CH_3COCH_2OH + H, \quad (3)$$

where the intermediate ion $CH_3COOH_2{}^+$ can be formed through two ion-molecule reactions $CH_3CO^+ + H_2O \longrightarrow CH_3COOH_2{}^+$, and $CH_3OH_2{}^+ + HCOOH \longrightarrow CH_3COOH_2{}^+ + H_2O$, as proposed in Remijan et al. (2002).

5 CONCLUSIONS

We present ALMA Band 4 observations of hydroxyacetone (CH_3COCH_2OH) toward IRAS 16293–2422 B. We have identified the molecular transitions and calculated physical parameters under LTE assumption. Main findings in this work are summarized below:

1. Totally 11 unblended transitions of CH_3COCH_2OH with upper level energies ranging from 86 to 246 K are identified in I16293B. It can be claimed as the first unambiguous detection of this molecule in interstellar space.
2. A rotational temperature of 160±21 K and a column density of $(1.2\pm1.0)\times10^{16}$ cm^{-2} have been obtained for CH_3COCH_2OH by using the LTE model. The compact gas distribution of CH_3COCH_2OH is coincident with the continuum emission of source B, which shows that this molecule is probably originated from the inner region near the hot corino of I16293B.
3. As a structural analogy of glycolaldehyde ($HCOCH_2OH$), we propose a similar reaction route to produce hydroxyacetone that it might be formed upon recombination of two free radicals CH_2OH and CH_3CO on the grain surface at low temperature. In the gas phase, the $CH_3COOH_2{}^+$ and CH_3OH reaction, followed by an electron recombination, to produce hydroxyacetone are proposed in our work.

Appendix A: LINES OF HYDROXYACETONE

For a proper identification, all transitions presented in the JPL catalog of molecule CH_3COCH_2OH at Band 4 were contained in our LTE synthetic spectrum. The frequencies of transitions with lower peak intensities than 3σ are presented in Table A.1.

Appendix B: FULL BAND SPECTRA

To make sure that the spectral models are reliable, we added full source model fitting. All published species in

Table A.1 Transitions of Hydroxyacetone with Weak Intensities ($<3\sigma$) at Band 4 toward I16293B

Rest Frequency (MHz)	Rest Frequency (MHz)	Rest Frequency (MHz)	Rest Frequency (MHz)	Rest Frequency (MHz)
145223.0	145282.9	145286.9	145293.4	145381.9
145438.3	145500.5	145518.0	145642.1	145666.7
145689.3	145744.1	145780.8	145796.6	145800.3
145803.2	145858.6	145913.8	145986.6	146237.4
146346.3	146364.4	146375.2	146411.6	146460.5
146472.6	146486.4	146556.8	146649.2	146710.2
146777.9	146814.4	146868.2	146886.0	146932.5
146935.2	146963.6	147040.7	147049.0	147068.9
147095.1	147158.4	147169.3	147172.4	147185.9
156950.2	156954.2	156958.1	157012.8	157185.7
157264.2	157330.9	157442.4	157461.9	157582.4
157635.9	157642.1	157773.0	157793.2	157803.8
157811.9	157852.7	157875.6	157889.2	157930.7
157986.4	158002.9	158024.5	158049.7	158080.1
158132.3	158170.4	158178.5	158183.5	158257.0
158424.9	158449.5	158451.1	158487.2	158518.1
158524.9	158613.0	158640.8	158644.8	158719.9
158841.3	158848.2	158954.0	158997.1	159013.8
159146.0				

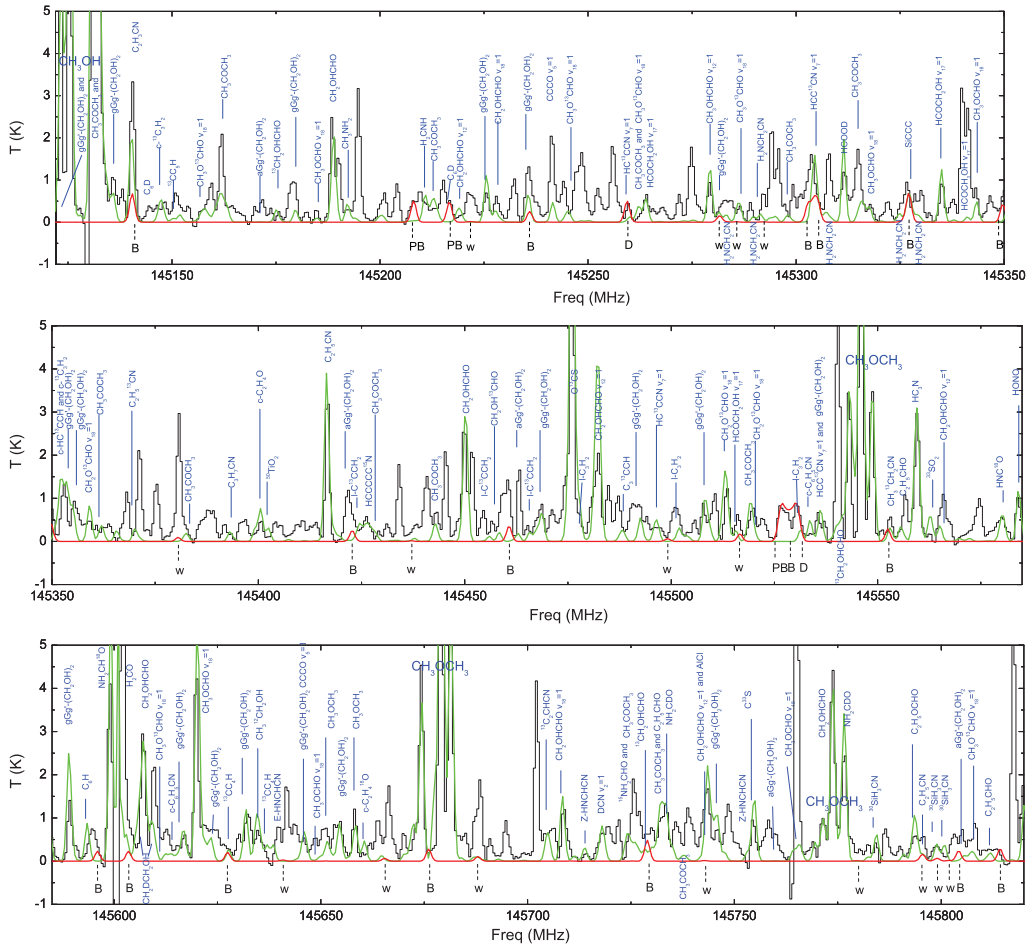

Fig. B.1 Full band spectra and line identification. The *black curve* is the observed data. XCLASS synthesized spectra of CH_3COCH_2OH is coded in *red color*. The detected unblended transitions are denoted with "D". The transitions partially blended with near molecules are denoted with "PB". The transitions totally blended with other molecules are denoted with "B". The transitions with weak intensities ($<3\sigma$) are denoted with "w". The *solid green curve* presents full source model spectra.

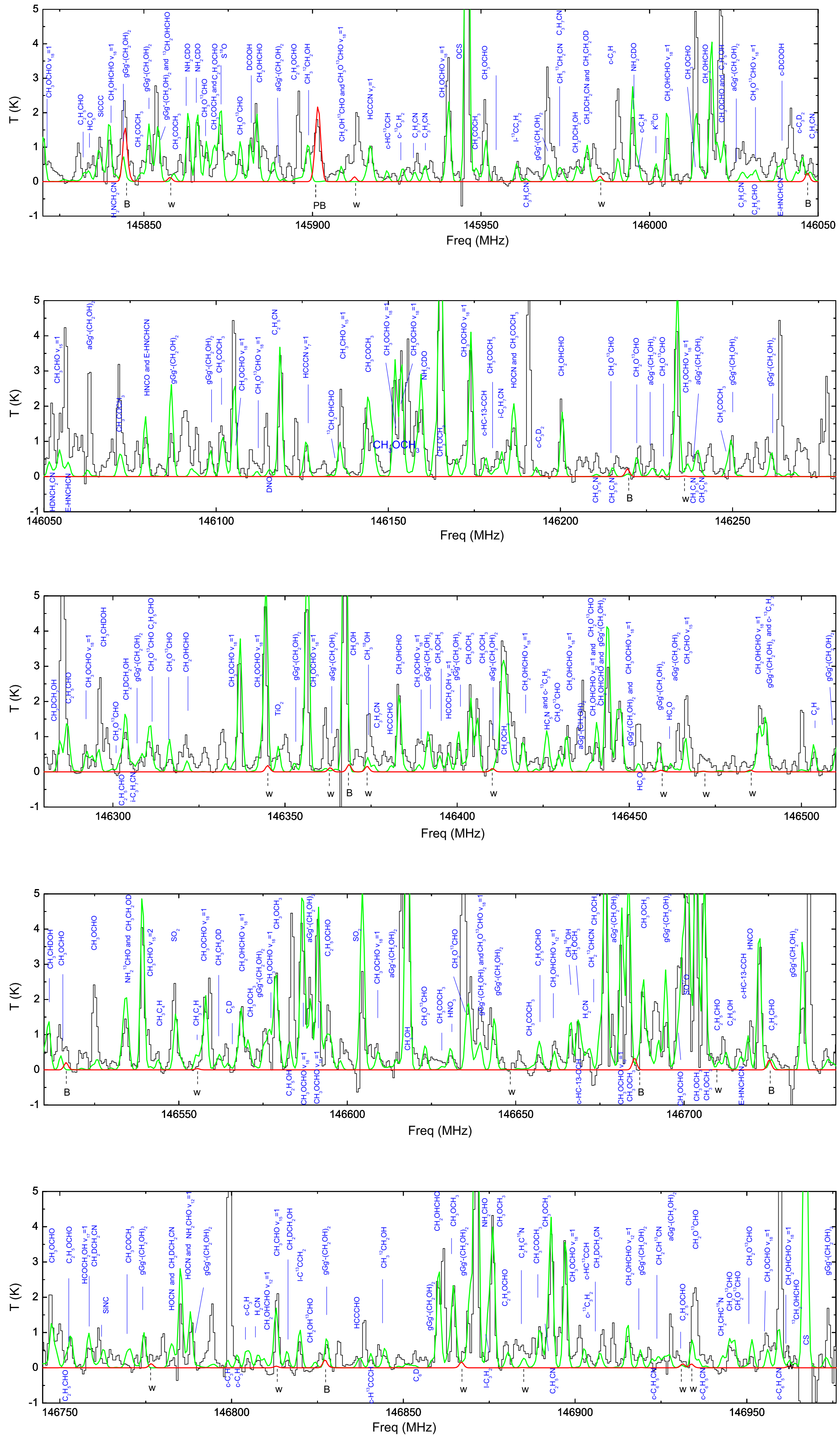

Fig. B.1 *Continued.*

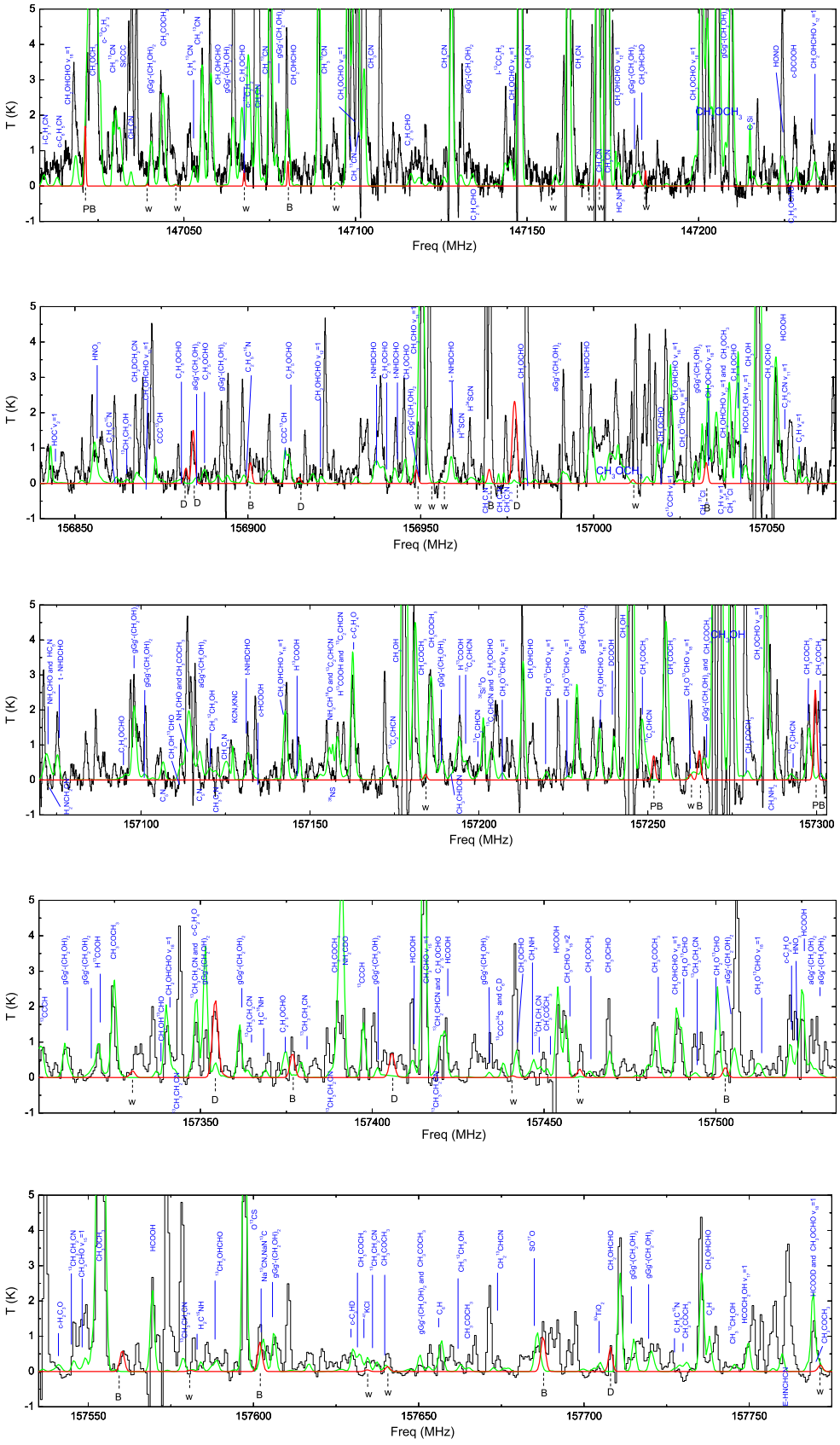

Fig. B.1 *Continued.*

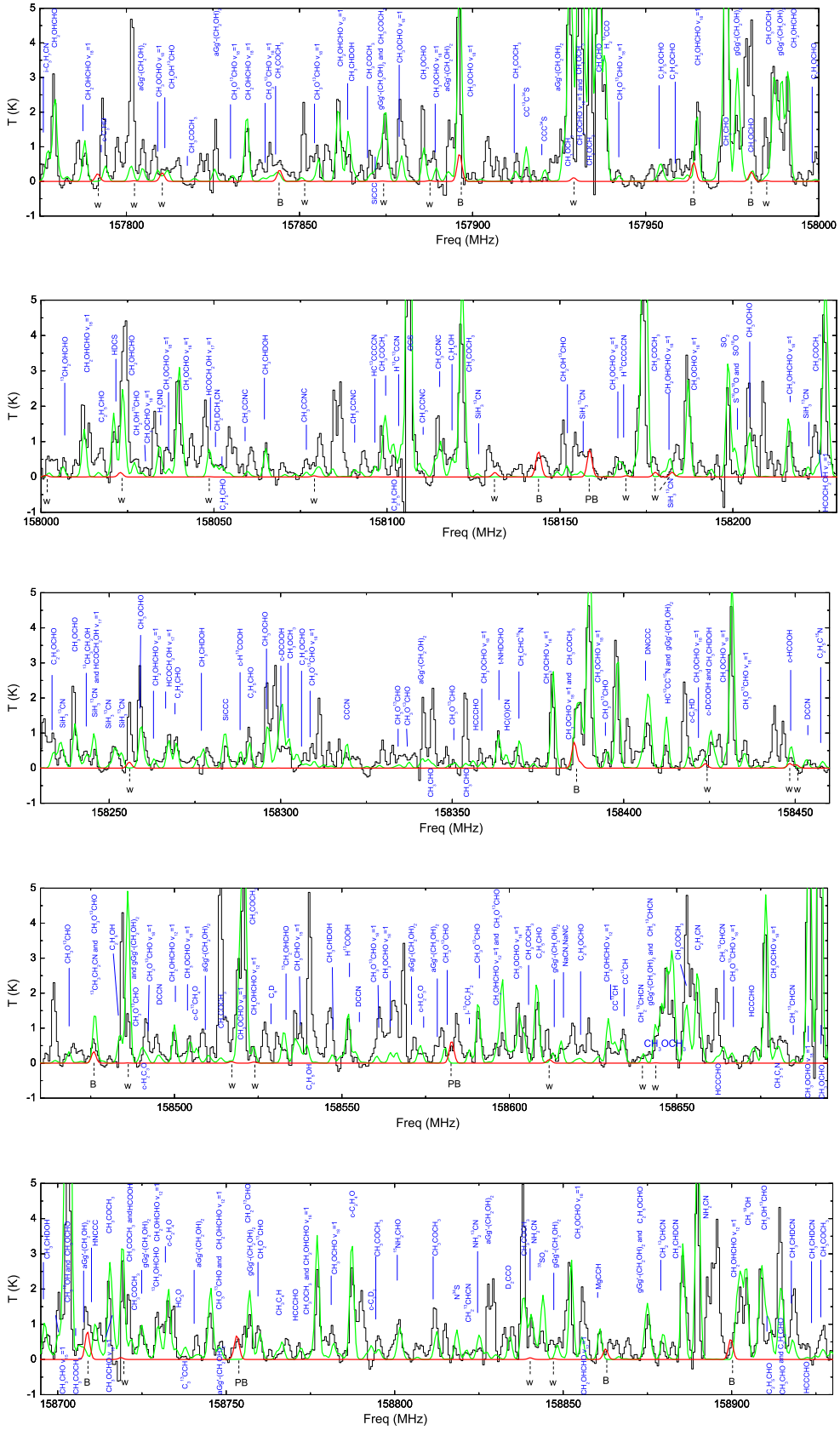

Fig. B.1 *Continued.*

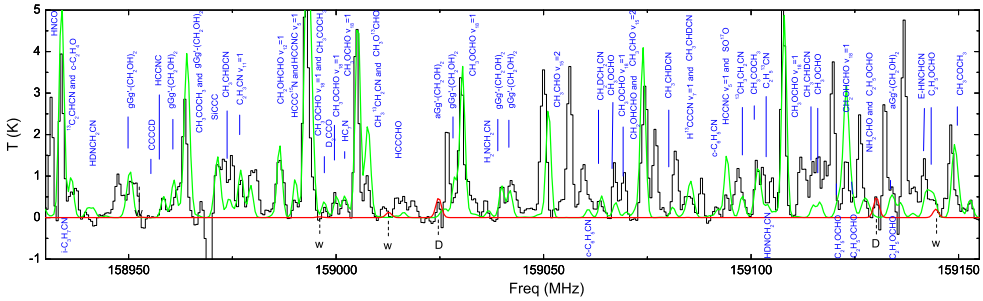

Fig. B.1 *Continued.*

source B, which are explicitly listed in recently work by Drozdovskaya et al. (2019) have been included. The full source model is shown with a solid green line in Figure B.1.

Acknowledgements S.-L. Qin is supported by the National Key R&D Program of China (No. 2017YFA0402701), by the Joint Research Fund in Astronomy (U1631237) under a cooperative agreement between the National Natural Science Foundation of China (NSFC) and the Chinese Academy of Sciences (CAS), and by the Top Talents Program of Yunnan Province (2015HA030). This work is also supported by the NSFC (Grant No. 11973075).

References

Alonso, E. R., McGuire, B. A., Kolesniková, L., et al. 2019, ApJ, 883, 18
Apponi, A. J., Halfen, D. T., Ziurys, L. M., et al. 2006a, ApJ, 643, L29
Apponi, A., Hoy, S., Halfen, D., Ziurys, L., & Brewster, M. 2006b, ApJ, 652, 1787
Beltrán, M. T., Codella, C., Viti, S., Neri, R., & Cesaroni, R. 2009, ApJ, 690, L93
Bergantini, A., Zhu, C., & Kaiser, R. I. 2018, ApJ, 862, 140
Bisschop, S. E., Jørgensen, J. K., Bourke, T. L., Bottinelli, S., & van Dishoeck, E. F. 2008, A&A, 488, 959
Biver, N., Bockelée-Morvan, D., Moreno, R., et al. 2015, Science Advences, 1, e1500863
Bossa, J. B., Ordu, M. H., Müller, H. S. P., Lewen, F., & Schlemmer, S. 2014, A&A, 570, A12
Braakman, R., Drouin, B., Widicus Weaver, S., & Blake, G., 2010, Journal of Molecular Spectroscopy, 264, 43
Butscher, T., Duvernay, F., Theule, P., et al. 2015, MNRAS, 453, 1587
Calcutt, H., Viti, S., Codella, C., et al. 2014, MNRAS, 443, 3157
Calcutt, H., Fiechter, M. R., et al. 2018, A&A, 617, A95
Caux, E., Kahane, C., Castets, A., et al. 2011, A&A, 532, A23
Cazaux, S., Tielens, A. G. G. M., Ceccarelli, C., et al. 2003, ApJ, 593, L51
Chuang, K. J., Fedoseev, G., Ioppolo, S., van Dishoeck, E. F., & Linnartz, H. 2016, MNRAS, 455, 1702
Cooper, G., Kimmich, N., Belisle, W., et al. 2001, Nature, 414, 879
Coutens, A., Ligterink, N. F. W., Loison, J.-C., et al. 2019, A&A, 623, L13
Coutens, A., Persson, M. V., Jørgensen, J. K., Wampfler, S. F., & Lykke, J. M. 2015, A&A, 576, A5
Drozdovskaya, M. N., van Dishoeck, E. F., Rubin, M., Jørgensen, J. K., & Altwegg, K. 2019, MNRAS, 490, 50
Fedoseev, G., Chuang, K. J., Ioppolo, S., et al. 2017, ApJ, 842, 52
Fedoseev, G., Cuppen, H. M., Ioppolo, S., Lamberts, T., & Linnartz, H. 2015, MNRAS, 448, 1288
Fuente, A., Cernicharo, J., Caselli, P., et al. 2014, A&A, 568, A65
Garrod, R. T. 2013, ApJ, 765, 60
Halfen, D. T., Apponi, A. J., Woolf, N., Polt, R., & Ziurys, L. M. 2006, ApJ, 639, 237
Hollis, J. M., Jewell, P. R., Lovas, F. J., & Remijan, A. 2004a, ApJ, 613, L45
Hollis, J. M., Jewell, P. R., Lovas, F. J., Remijan, A., & Møllendal, H. 2004b, ApJL, 610, L21
Hollis, J. M., Lovas, F. J., & Jewell, P. R. 2000, ApJ, 540, L107
Hollis, J. M., Vogel, S. N., Snyder, L. E., Jewell, P. R., & Lovas, F. J. 2001, ApJ, 554, L81
Iozzo, R. V. 1998, Annu. Rev. Biochem., 67, 609
Jørgensen, J. K., Bourke, T. L., Nguyen Luong, Q., & Takakuwa, S. 2011, A&A, 534, A100
Jørgensen, J. K., Favre, C., Bisschop, S. E., et al. 2012, ApJ, 757, L4
Jørgensen, J. K., van der Wiel, M. H. D., & Coutens, A. 2016, A&A, 595, A117
Jørgensen, J. K., et al. 2018, A&A, 620, A170
Kattija-Ari, M., & Harmony, M. 1980, Internaltion Journal of Quantum Chemistry: Quantum Chemistry Symposium 14, 18, 443
Kolesniková, L., Peña, I., Alonso, E. R., et al. 2018, A&A, 619, A67
Lis, D. C., Carlstrom, J. E., & Keene, J. 1991, ApJ, 380, 429

Lykke, J. M., Coutens, A., Jørgensen, J. K., et al. 2017, A&A, 597, A53
Martín-Doménech, R., Rivilla, V. M., Jiménez-Serra, I., et al. 2017, MNRAS, 469, 2230
Michael, J. V., Nava, D. F., Payne, W. A., & Stief, L. J. 1979, Chem. Phys., 70, 5222
Mohăcek-Groše, V. 2005, Spectrochimica Acta Part A, 61, 477
Möller, T., Endres, C., & Schilke, P. 2017, A&A, 598, A7
Müller, H. S. P., Schlöder, E., Stutzki, J., & Winnewisser, G. 2005, Journal of Molecular Structure, 742, 215
Müller, H. S. P., Thorwirth, S., Roth, D. A., & Winnewisser, G. 2001, A&A, 370, L49
Öberg, K. I., Garrod, R. T., van Dishoeck, E. F., & Linnart, H. 2009, A&A, 504, 891
Pickett, H. M., Poynter, R. L., & Cohen, E. A. 1998, Cohen, J. Quant. Spectr. Rad. Transf., 60, 883
Qin, S.-L., Wu, Y., Huang, M., et al. 2010, ApJ, 711, 399
Redondo, P., Martínez, H., Largo, A., & Barrientos, C. 2017, A&A, 603, A139
Remijan, A., Snyder, L. E., Liu, S.-Y., et al. 2002, ApJ, 576, 264
Requena-Torres, M. A., Martín-Pintado, J., Martín, S., et al. 2008, ApJ, 672, 352
Ruaud, M., Loison, J. C., Hickson, K. M., et al. 2015, MNRAS, 447, 4004
Sánchez-Monge, Á., Schilke, P., Ginsburg, A., et al. 2018, A&A, 609, A101
Solomons, T. W. G. 1984, Organic Chemistry (3rd ed.; New York: Wiley)
Taquet, V., López-Sepulcre, A., Ceccarelli, C., et al. 2015, ApJ, 804, 81